Preparation and Characterization of Nanocomposites Based on Polylactides Tethered with Polyhedral Oligomeric Silsesquioxane

Jong Hyun Lee, Young Gyu Jeong

School of Advanced Materials and System Engineering, Kumoh National Institute of Technology, Gumi 730-701, Republic of Korea

Received 19 February 2009; accepted 4 July 2009
DOI 10.1002/app.31076
Published online 15 September 2009 in Wiley InterScience (www.interscience.wiley.com).

ABSTRACT: A series of polylactides tethered with polyhedral oligomeric silsesquioxane (POSS–PLAs) were synthesized via the ring-opening polymerization of L-lactide with 3-hydroxypropylheptaisobutyl polyhedral oligomeric silsesquioxane (3-hydroxypropylheptaisobutyl POSS) at a concentration of 0.02–2.00 mol % in the presence of a stannous(II) octoate catalyst. ^{1}H-NMR spectra and a composition analysis of the POSS–PLA hybrids confirmed that 3-hydroxypropylheptaisobutyl POSS served as an initiator for L-lactide in the ring-opening polymerization. X-ray diffraction patterns evidenced that polyhedral oligomeric silsesquioxane (POSS) molecules of POSS–PLA hybrids were well dispersed without the formation of their crystalline aggregates. The POSS–PLA hybrid with 0.50 mol % POSS content was solution-blended with a neat polylactide (PLA) homopolymer to obtain PLA/POSS–PLA nanocomposites with various POSS–PLA contents of 1–30 wt %. The X-ray diffraction results of the PLA/POSS–PLA nanocomposites demonstrated that the POSS–PLA was well dispersed in the neat PLA matrix. The thermal and thermooxidative degradation properties of the nanocomposites were found to be improved at POSS–PLA contents of 1–20 wt %, compared to the neat PLA. The crystallization rates and crystallinities of the PLA/POSS–PLA nanocomposites were faster and higher, respectively, with increasing POSS–PLA content because of the nucleation effect of the POSS molecules in the neat PLA matrix. © 2009 Wiley Periodicals, Inc. J Appl Polym Sci 115: 1039–1046, 2010

Key words: nanocomposites; reinforcement; ring-opening polymerization; structure-property relations; thermal properties

INTRODUCTION

Recently, much attention has been paid to polylactides (PLAs) as environmentally friendly, biocompatible, and biodegradable thermoplastic polymers. They have been used as biomedical materials, packaging films, fibers, and thermoplastics in various applications.[1,2] Although PLAs exhibit excellent transparency, compostibility, and thermal and mechanical properties, their weakness in thermal stability, toughness, and dimensional stability limits their application. Therefore, several studies have been carried out to overcome the disadvantages of long-term applications of PLA by the introduction of nanoparticles such as nanoclays and carbon nanotubes into the PLA matrix.[3–8]

Among nanoparticles, polyhedral oligomeric silsesquioxanes (POSSs) are a class of versatile building blocks for the preparation of organic–inorganic hybrid polymers with designed properties.[9–11] The chemical composition of POSS is a hybrid intermediate ($RSiO_{1.5}$) between molecules of silica (SiO_2) and silicones (R_2SiO), and its size is nanoscopic, ranging from 1 to 3 nm. Accordingly, POSS nanoparticles with tailored and well-defined structures have been extensively used to modify various thermal and mechanical properties of organic polymers at the molecular level.[12–22]

It is known that hydroxyl-containing initiators such as 1-octanol are used to control the molecular weight and accelerate the ring-opening polymerization reaction of lactide monomers.[22,23,24] Therefore, we expected that hydroxyl-containing POSS molecules could be adopted as initiators in the ring-opening polymerization of lactide to achieve enhanced physical properties in PLA. In a similar study, it was recently reported that an amino-functionalized POSS was used as the initiator of the ring-opening polymerization of caprolactone and lactide to obtain organic–inorganic nanohybrids.[25]

In this study, for the first time, we synthesized a series of polylactides tethered with polyhedral oligomeric silsesquioxane (POSS–PLAs) via the ring-opening polymerization of L-lactide with 3-hydroxypropylheptaisobutyl POSS as an initiator in the presence of a stannous(II) octoate [$Sn(Oct)_2$]

Correspondence to: Y. G. Jeong (ygjeong@kumoh.ac.kr).
Contract grant sponsor: National Research Foundation of Korea Grant (Ministry of Education, Science, and Technology); contract grant number: KRF-2007-331-D00567.

© 2009 Wiley Periodicals, Inc.

TABLE I
Compositions and Molecular Weights of POSS-PLA Hybrids

Sample code	Feed composition of the POSS initiator (mol %)	Composition of the POSS initiator determined by ^{1}H-NMR (mol %)	Feed molar ratio of lactide to the POSS initiator	M_n (g/mol)
POSS–PLA 0.02	0.02	0.07	5000	67,200
POSS–PLA 0.05	0.05	0.09	2000	54,300
POSS–PLA 0.10	0.10	0.15	1000	37,400
POSS–PLA 0.20	0.20	0.20	500	18,900
POSS–PLA 0.50	0.50	0.45	200	11,900
POSS–PLA 1.00	1.00	0.85	100	6,100
POSS–PLA 2.00	2.00	1.76	50	2,700

catalyst and introduced the POSS–PLA hybrid into a commercially available neat PLA homopolymer to prepare PLA/POSS–PLA nanocomposites. The chemical structures and molecular compositions of the synthesized POSS–PLA hybrids were characterized by ^{1}H-NMR spectroscopy. The structures, thermooxidative stability, and thermal and mechanical properties of the PLA/POSS–PLA nanocomposites were also investigated by X-ray diffraction, differential scanning calorimetry (DSC), thermogravimetric analysis (TGA), and tensile experiments, respectively.

EXPERIMENTAL

Materials

L-Lactide (99.5%, Purac Co., Amsterdam, Netherlands) was used as the monomer for ring-opening polymerization. 3-Hydroxypropylheptaisobutyl POSS (Sigma–Aldrich Co., St. Louis, MO), a hydroxyl-containing POSS, was used as the initiator of L-lactide. $Sn(Oct)_2$ (Sigma–Aldrich) was adopted as a catalyst for the ring-opening polymerization of L-lactide. A commercially available neat PLA homopolymer [model 4032D, number-average molecular weight (M_n) $\approx 3 \times 10^4$ g/mol, D-isomer content = 1 mol %] was supplied by NatureWorks LLC (Minnetonka, MN). All of the chemicals and materials were used without further purification.

Synthesis of the POSS–PLA hybrids by ring-opening polymerization

Dozens of gram-scale POSS–PLAs were synthesized via the ring-opening polymerization of L-lactide with the 3-hydroxypropylheptaisobutyl POSS initiator and $Sn(Oct)_2$ catalyst at 180°C for 90 min. The melt-state polymerization was performed in a custom-designed glassware reactor. The composition of the POSS initiator for the synthesis of the POSS–PLA hybrids was controlled to be 0.02–2.0 mol %, as listed in Table I, and the monomer-to-catalyst ratio {[Lactide]/[$Sn(Oct)_2$]} was kept constant at 5000/1. The overall reaction scheme is shown in Figure 1. We terminated the polymerization reaction by quenching the product in iced water. The final products were purified by dissolution in chloroform, precipitation into methanol, and filtration. The purified products were then dried *in vacuo* at 50°C for at least 24 h.

Preparation of the PLA/POSS–PLA nanocomposites

A series of PLA/POSS–PLA nanocomposites were prepared by the solution mixing of the neat PLA homopolymer and POSS–PLA 0.50 hybrid. The

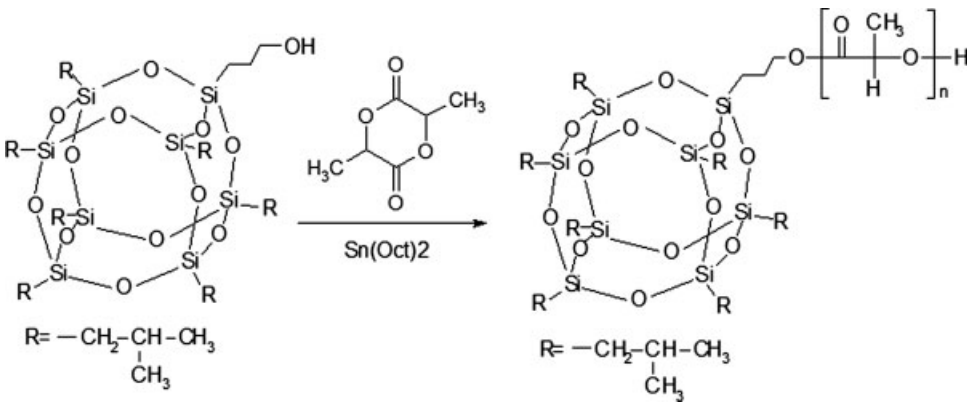

Figure 1 Scheme for synthesizing POSS–PLA hybrids via the ring-opening polymerization of L-lactide with 3-hydroxylpropylheptaisobutyl POSS as the initiator in the presence of $Sn(Oct)_2$.

mixture (10 g) of the neat PLA and POSS–PLA 0.50 hybrid was dissolved in 200 mL of chloroform. The content of the POSS–PLA 0.50 hybrid in the PLA/POSS–PLA nanocomposites was adjusted to be 1–30 wt %. The solutions were precipitated into excess methanol, and the precipitates were filtered. The PLA/POSS–PLA filtrates were washed with methanol several times and then dried *in vacuo* at 50°C for 24 h. The nanocomposites were named PLA/POSS–PLA *x*, where *x* denotes the weight percentage of POSS–PLA.

Characterization of the POSS–PLA hybrids and PLA/POSS–PLA nanocomposites

The chemical structures and compositions of the POSS–PLA hybrids were characterized with an ^{1}H- NMR spectrometer (Bruker, Ettlingen, Germany, 400 MHz). The samples were dissolved in a $CDCl_3$ solvent with tetramethylsilane (TMS) as the internal reference.

The X-ray diffraction patterns of the POSS–PLA hybrids and PLA/POSS–PLA nanocomposites were obtained with a Rigaku (Tokyo, Japan) X-ray diffractometer (Ni-filtered Cu Kα radiation, 40 kV and 200 mA) at a scanning rate of 2.0°/min.

To examine the dispersion of the POSS–PLA hybrids in the PLA homopolymer matrix by comparison of the optical clarity or transparency of the nanocomposites with various POSS–PLA hybrid contents, optical images of the neat PLA homopolymer and PLA/POSS–PLA nanocomposites were obtained with a digital camera.

The thermal and thermooxidative stability of the PLA/POSS–PLA nanocomposites was characterized with a thermogravimetric analyzer (TGA Q500, TA Instruments, New Castle, DE) at a heating rate of 20°C/min under a nitrogen or oxygen gas atmosphere.

The thermal properties of the samples were measured by DSC (Diamond DSC, PerkinElmer, Inc., Waltham, MA). All measurements were performed at a heating rate of 10°C/min under nitrogen gas conditions. The exothermic and endothermic peak temperatures of the heating thermograms were taken as the apparent crystallization and melting temperatures, respectively. The onset temperatures of glass transition were considered to be the glass-transition temperatures.

The mechanical properties of the PLA/POSS–PLA nanocomposites, such as the tensile strength and modulus, were measured with a universal testing machine (Instron series 4467, Norwood, MA) according to ASTM D 638-00. The gauge length was 5 cm, and the crosshead speed was 1 cm/min.

For the X-ray diffraction, optical clarity, DSC, TGA, and tensile experiments, melt-quenched amorphous PLA/POSS–PLA nanocomposite films (~0.2 mm thick) were prepared by compression molding in a hot press at 190°C for 3 min, quenching into iced water, and drying *in vacuo* at room temperature for 24 h.

RESULTS AND DISCUSSION

Structures and characterization of the POSS–PLA hybrids

The ^{1}H-NMR spectra of the 3-hydroxypropylheptaisobutyl POSS initiator, POSS–PLA 2.0 hybrid, and neat PLA homopolymer with peak assignments are shown in Figure 2. Because the peaks corresponding to the protons of the PLA backbone chains (*h* and *g*) were separated clearly from those of the POSS initiator (*a* and *c* + *d*), the POSS content of the synthesized POSS–PLA hybrids were quantitatively calculated with the following equation:

$$\frac{a}{42h} = \frac{a}{14g} = \frac{y}{x},\ x + y = 1 \tag{1}$$

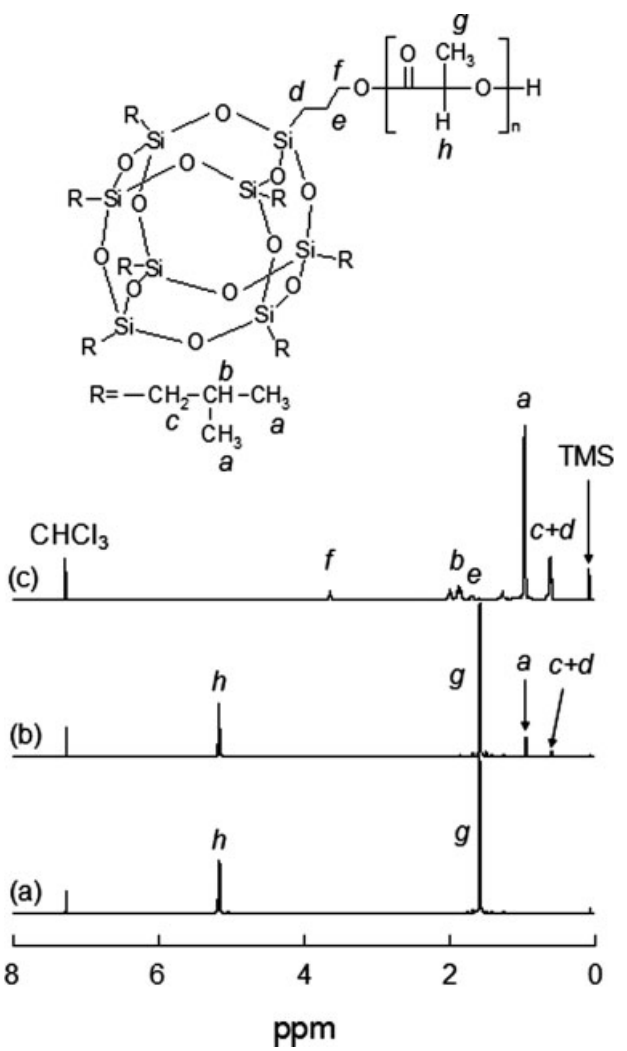

Figure 2 ^{1}H-NMR spectra of (a) the neat PLA homopolymer, (b) the POSS–PLA 0.50 hybrid, and (c) the 3-hydroxylpropylheptaisobutyl POSS initiator.

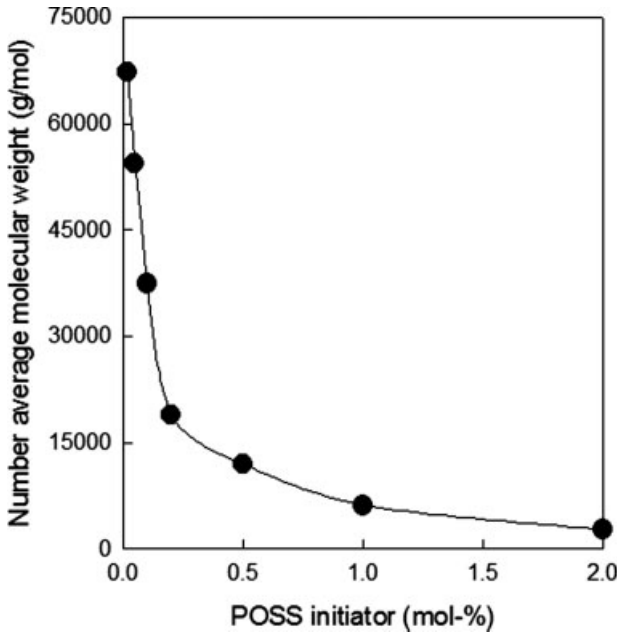

Figure 3 M_n of POSS–PLA hybrids prepared by the ring-opening polymerization of L-lactide with various contents of 3-hydroxylpropylheptaisobutyl POSS.

where x and y indicate the molar fractions of the POSS and PLA repeating units, respectively. When the POSS contents of the POSS–PLA hybrids calculated by eq. (1) were compared with the feed compositions, they were found to be slightly higher than the feed compositions, as listed in Table I. In addition, M_n of the PLA chains in the POSS–PLA hybrids could be evaluated from the ratio of y to x, as summarized in Table I. M_n of the POSS–PLA hybrids exponentially decreased with increasing feed composition of the POSS initiator, as shown in Figure 3. This showed that the 3-hydroxylpropylheptaisobutyl POSS served as an efficient initiator for the L-lactide monomer in the ring-opening polymerization.

Figure 4 represents the X-ray diffraction patterns of the POSS–PLA hybrids and hydroxyl-functionalized POSS initiator. Although 3-hydroxylpropylheptaisobutyl POSS displayed sharp crystalline diffractions, all of the POSS–PLA hybrids exhibited only amorphous hallow scattering patterns, which demonstrated that the POSS molecules tethered on the PLA chains were well dispersed in the POSS–PLA hybrids without the formation of their crystalline phases or aggregates.

Structures and thermal and mechanical properties of the PLA/POSS–PLA nanocomposites

The PLA/POSS–PLA nanocomposites were prepared by the solution mixing of the neat PLA homopolymer with 1–30 wt % of the POSS–PLA 0.50 hybrid. Figure 5 shows the wide-angle X-ray diffraction patterns of the melt-quenched neat PLA and PLA/POSS–PLA film samples. For all of the PLA/POSS–PLA nanocomposites, the crystalline diffraction peaks of the POSS nanoparticles were not detected, which dictated that the POSS molecules capped on POSS–PLA were well dispersed in the neat PLA matrix.

Figure 6(A–F) displays the optical images of the melt-quenched neat PLA homopolymer and PLA/POSS–PLA nanocomposite films, which were obtained to confirm the uniform dispersion of the POSS–PLA hybrids in the nanocomposites. All of the PLA/POSS–PLA nanocomposites were optically transparent without showing any heterogeneity, regardless of the POSS–PLA contents. This supported the fact that the POSS–PLA hybrids were well dispersed in the neat PLA matrix. For comparison, optical images of the PLA/POSS composites, which were prepared by mixture of the neat PLA homopolymer with 5 and 10 wt % of the 3-hydroxylpropylheptaisobutyl POSS, were obtained, as shown in Figure 6(G,H). As a result, the PLA/POSS composites were found to become opaque with increasing POSS content; this indicated that the POSS molecules were not well dispersed in the PLA matrix by the formation of the aggregates, unlike in the

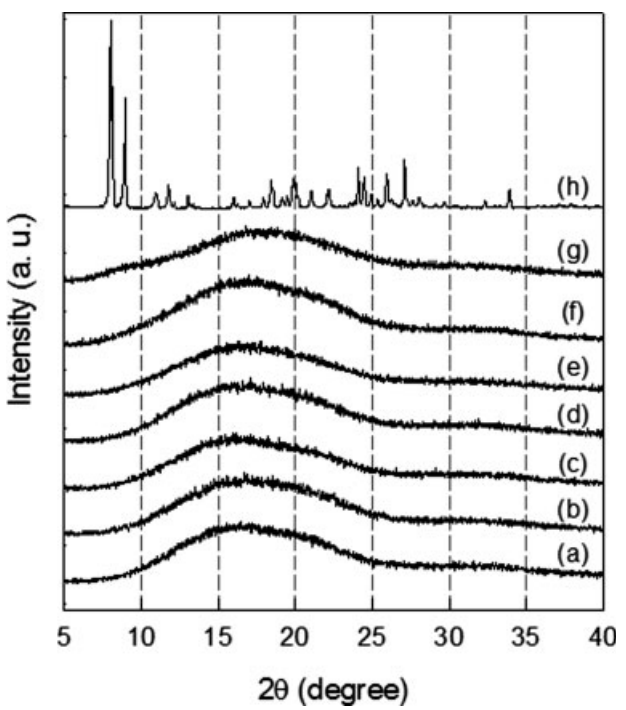

Figure 4 X-ray diffraction patterns of 3-hydroxylpropylheptaisobutyl POSS and POSS–PLA hybrids: (a) POSS–PLA 0.02, (b) POSS–PLA 0.05, (c) POSS–PLA 0.10, (d) POSS–PLA 0.20, (e) POSS–PLA 0.50, (f) POSS–PLA 1.00, (g) POSS–PLA 2.00, and (h) 3-hydroxylpropylheptaisobutyl POSS.

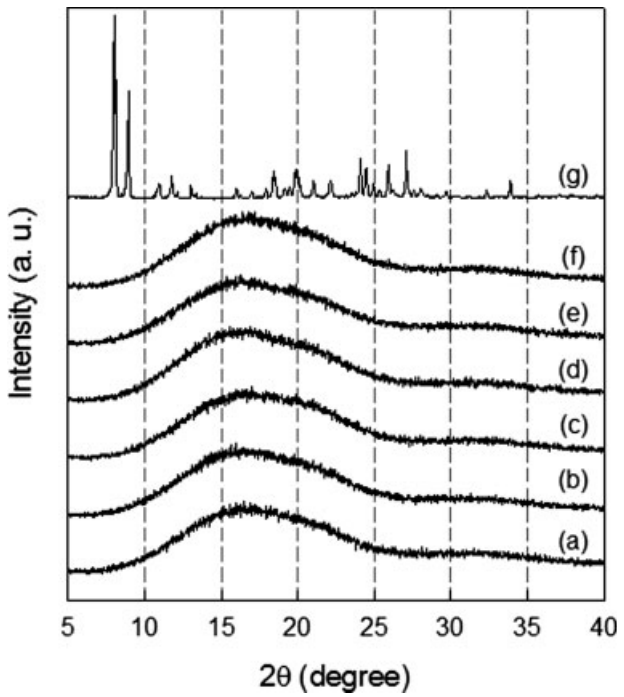

Figure 5 X-ray diffraction patterns of the melt-quenched amorphous neat PLA homopolymer and PLA/POSS–PLA nanocomposites: (a) neat PLA, (b) PLA/POSS–PLA 1, (c) PLA/POSS–PLA 5, (d) PLA/POSS–PLA 10, (e) PLA/POSS–PLA 20, (f) PLA/POSS–PLA 30, and (g) 3-hydroxylpropylheptaisobutyl POSS.

PLA/POSS–PLA nanocomposites. Therefore, it was valid to conclude that for the PLA/POSS–PLA nanocomposites, the homogeneous dispersion of the POSS–PLA hybrids in the PLA matrix was due to the miscibility of the PLA chains of the POSS–PLA hybrids with the neat PLA homopolymer.

Figure 7 shows the TGA curves of the neat PLA and PLA/POSS–PLA nanocomposite films examined under an inert nitrogen gas atmosphere. The thermal decomposition temperatures for 5 and 50% weight loss were evaluated from the TGA curves, as listed in Table II. Overall, the thermal stabilities of the PLA/POSS–PLA nanocomposites with POSS–PLA 0.50 hybrid contents of 1–20 wt % were found to be higher than that of the neat PLA homopolymer. This result originated from the fact that the POSS molecules tethered on the POSS–PLA hybrids might have served as barriers to minimize the permeability of volatile degradation products from the material, eventually leading to a delay in the thermal degradation of PLA/POSS–PLA nanocomposites. On the other hand, the thermal degradation temperatures decreased slightly with the increment of the POSS–PLA 0.50 hybrids from 1 to 30 wt %. Finally, the thermal decomposition temperatures of the PLA/POSS–PLA 30 nanocomposite were somewhat lower than those of the neat PLA homopolymer. We expect that the POSS molecules tethered on PLA chains contributed to the enhanced thermal degradation properties of the PLA/POSS–PLA nanocomposites, whereas the low molecular weight of POSS–PLA compared to the neat PLA matrix deteriorated the thermal stability of the nanocomposites. In other words, the lower molecular weight effect of POSS–PLA became dominant rather than the reinforcing effect of the POSS molecules, as the POSS–PLA content increased in the nanocomposites. As the result, at the higher POSS–PLA content of 30 wt %, the reinforcing effect of the POSS molecules could be offset by the lower molecular weight of POSS–PLA in the PLA/POSS–PLA nanocomposites.

The TGA curves of the neat PLA and PLA/POSS–PLA nanocomposites films examined in an oxygen gas atmosphere are presented in Figure 8. The TGA curves under an oxygen atmosphere (Fig. 8) were quite different from those under inert nitrogen gas conditions (Fig. 7) because oxygen played an important role in the thermooxidative degradation of the neat PLA homopolymer and POSS–PLA nanocomposites. As a result, the thermooxidative degradation temperatures for 5 and 50% weight loss of the neat PLA and POSS–PLA nanocomposites under the oxygen gas conditions were somewhat lower than those

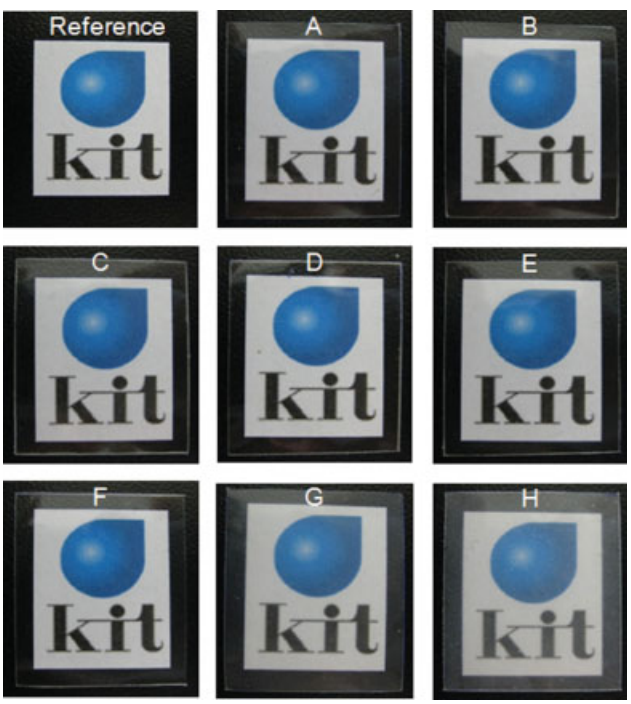

Figure 6 Optical images of the melt-quenched neat PLA homopolymer and PLA/POSS–PLA nanocomposites: (A) neat PLA, (B) PLA/POSS–PLA 1, (C) PLA/POSS–PLA 5, (D) PLA/POSS–PLA 10, (E) PLA/POSS–PLA 20, and (F) PLA/POSS–PLA 30. (G,H) For comparison, optical images of PLA/POSS composites with POSS contents of 5 and 10 wt %, respectively, are shown. [Color figure can be viewed in the online issue, which is available at www.interscience.wiley.com.]

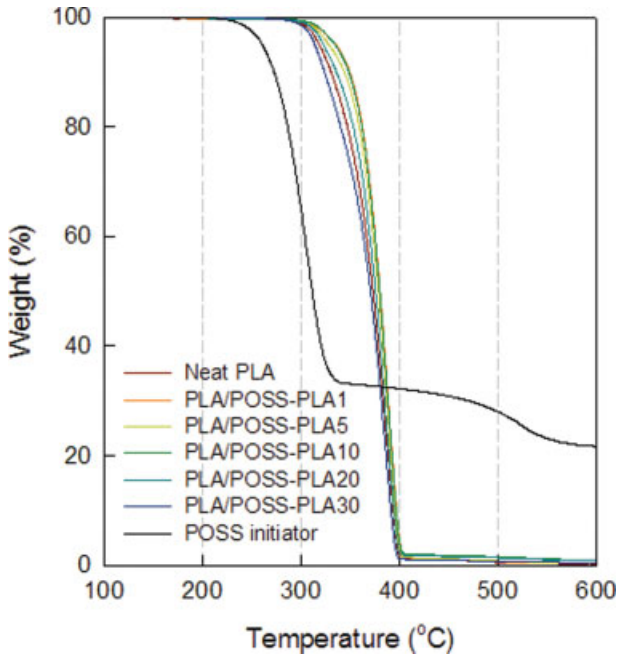

Figure 7 TGA curves of the neat PLA homopolymer and PLA/POSS–PLA nanocomposites tested under the nitrogen gas condition. [Color figure can be viewed in the online issue, which is available at www.interscience.wiley.com.]

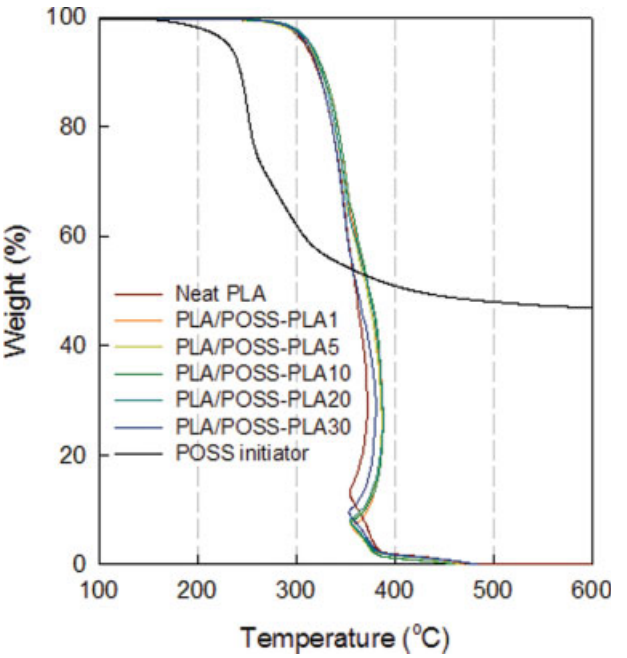

Figure 8 TGA curves of the neat PLA homopolymer and PLA/POSS–PLA nanocomposites tested under the oxygen gas condition. [Color figure can be viewed in the online issue, which is available at www.interscience.wiley.com.]

under the nitrogen gas conditions, as summarized in Table II. Nevertheless, the thermooxidative degradation temperatures of the PLA/POSS–PLA nanocomposites under the oxygen gas conditions were 2–15°C higher than those of the neat PLA homopolymer. This improvement in the thermooxidative stability was attributed to the formation of a silica layer on the surface of the PLA matrix, which served as a barrier preventing the further degradation of the underlying PLA matrix,[26,27] as noted previously. On the other hand, the thermooxidative degradation temperatures of the nanocomposites were not influenced by the POSS–PLA hybrid content, whereas the thermal degradation temperatures examined under a nitrogen gas atmosphere slightly decreased with increasing POSS–PLA hybrid content because of the deteriorating effect of the lower molecular weight of the POSS–PLA hybrid in the neat PLA matrix, as described previously. Therefore, we considered that the reinforcing effect of the POSS molecules of POSS–PLA on the thermal stability of the PLA/POSS–PLA nanocomposites was effective under an oxygen gas atmosphere rather than under nitrogen gas conditions. In addition, there was an unexpected temperature decrease in the TGA curves under the oxygen atmosphere, unlike in the curves under the nitrogen atmosphere. This unusual result might have been from the fact that the low molecules formed by the thermooxidative degradation under the oxygen atmosphere adsorbed thermal energy from the sample to evaporate, which led to a decrease in the overall sample temperature.

TABLE II
Thermal and Thermo-Oxidative Degradation Temperatures of PLA/POSS-PLA Nanocomposites Under the Nitrogen and Oxygen Gas Condition

	Nitrogen gas condition		Oxygen gas condition	
Sample code	$T_{0.05}$ (°C)	$T_{0.50}$ (°C)	$T_{0.05}$ (°C)	$T_{0.50}$ (°C)
Neat PLA	319	373	309	361
PLA/POSS–PLA 1	335	380	314	374
PLA/POSS–PLA 5	328	379	312	372
PLA/POSS–PLA 10	335	380	315	375
PLA/POSS–PLA 20	323	376	315	374
PLA/POSS–PLA 30	314	371	312	362
POSS initiator	261	311	231	420

$T_{0.05}$ = thermal decomposition temperature for 5% weight loss; $T_{0.50}$ = thermal decomposition temperature for 50% weight loss.

Figure 9 shows the DSC thermograms of the melt-quenched amorphous neat PLA homopolymer, POSS–PLA 0.50 hybrid, and PLA/POSS–PLA nanocomposites with various POSS–PLA 0.50 hybrid contents of 1–30 wt %. The cold-crystallization temperatures of the melt-quenched PLA/POSS–PLA nanocomposite films shifted to lower temperatures with increasing POSS content, as shown in Figure 9.

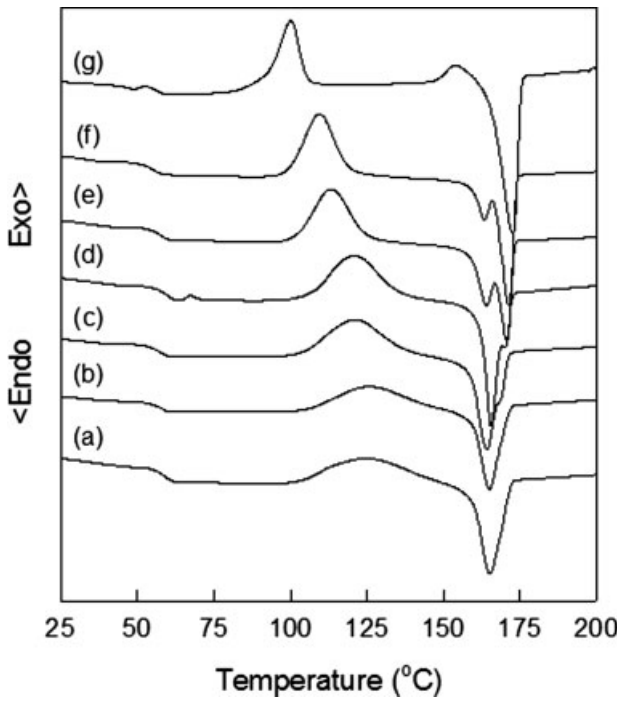

Figure 9 DSC heating thermograms of the melt-quenched amorphous film samples: (a) neat PLA, (b) PLA/POSS–PLA 1, (c) PLA/POSS–PLA 5, (d) PLA/POSS–PLA 10, (e) PLA/POSS–PLA 20, (f) PLA/POSS–PLA 30, and (g) POSS–PLA 0.50.

In addition, the crystallization exothermic peak area became higher with increasing POSS–PLA 0.50 hybrid content in the nanocomposites. This revealed that the crystallization rates of the nanocomposites increased with increasing POSS–PLA content because of the nucleation effect of the POSS molecules dispersed uniformly in the PLA matrix. This result was supported by the crystallization exothermic peak width, which became narrower with increasing POSS–PLA content in the PLA/POSS–PLA nanocomposites. On the other hand, the glass-transition temperatures of the PLA/POSS–PLA nanocomposites remained unchanged, regardless of the POSS–PLA content, as listed in Table III.

TABLE III
Thermal Transition Properties of the Melt-Quenched Amorphous Films of Neat PLA, PLA/POSS-PLA Nanocomposites, and POSS-PLA 0.50 Hybrid

Sample code	T_g (°C)	T_{cc} (°C)	ΔH_{cc} (J/g)	T_m (°C)	
				T_{m1}	T_{m2}
Neat PLA	55	124	32	165	—
PLA/POSS–PLA 1	54	125	36	165	—
PLA/POSS–PLA 5	53	124	36	164	169
PLA/POSS–PLA 10	56	121	39	165	171
PLA/POSS–PLA 20	53	113	34	164	171
PLA/POSS–PLA 30	54	109	37	164	171
POSS–PLA 0.50	54	100	28	—	173

ΔH_{cc} = cold-crystallization exothermic peak area; T_{cc} = cold-crystallization temperature; T_g = glass-transition temperature; T_m = melting temperature.

Uniaxial tensile experiments for the melt-quenched amorphous PLA homopolymer and PLA/POSS–PLA nanocomposite films were carried out at room temperatures. The resulting tensile strength at break and initial modulus values of the neat PLA and PLA/POSS–PLA nanocomposites were evaluated and are presented as a function of the POSS–

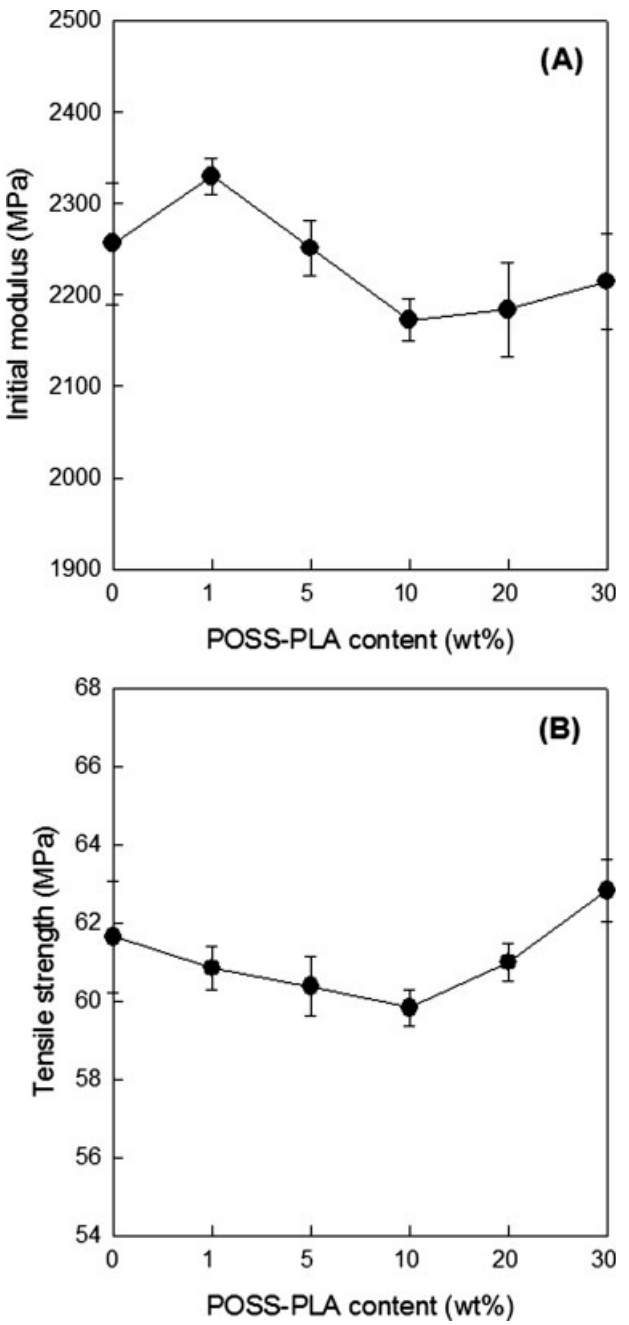

Figure 10 (A) Initial modulus and (B) tensile strength of the PLA/POSS–PLA nanocomposites as a function of the POSS–PLA content.

PLA 0.50 hybrid content, as shown in Figure 10. Overall, the initial modulus slightly increased at a POSS–PLA content of 1 wt % and decreased slightly at a higher POSS–PLA content [Fig. 10(A)]. We suppose that this change of initial moduli of the PLA/POSS–PLA nanocomposites with the POSS–PLA content originated from the competition of the reinforcing effect of POSS molecules dispersed in the PLA matrix and the chain slippage effect of the lower molecular weight of POSS–PLA in the matrix, as discussed previously. On the other hand, the tensile strength at break of the PLA/POSS–PLA nanocomposites as a function of POSS–PLA content was found to remain unchanged within the experimental error [Fig. 10(B)].

CONCLUSIONS

POSS–PLAs were successfully prepared by the ring-opening polymerization of L-lactide with 3-hydroxypropylheptaisobutyl POSS as an initiator in the presence of an $Sn(Oct)_2$ catalyst. ^{1}H-NMR spectra of the POSS–PLA hybrids confirmed that the hydroxyl-containing POSS molecule served as an initiator for the ring-opening polymerization of L-lactide, and it was quantitatively attached to the PLA chains. X-ray diffraction patterns evidenced that the POSS nanoparticles did not form crystalline aggregates in the POSS–PLA hybrids. PLA/POSS–PLA nanocomposites with various POSS–PLA contents of 1–30 wt % were prepared by the solution blending of a commercially available neat PLA homopolymer with a POSS–PLA hybrid with 0.50 mol % POSS. The X-ray diffraction patterns of the melt-quenched PLA/POSS–PLA nanocomposites confirmed that the POSS–PLA hybrid was well dispersed in the PLA matrix. Because of the compromising effects between the reinforcement of tethered POSS molecules and the low molecular weight of POSS–PLA in the PLA/POSS–PLA nanocomposites, the thermal and thermooxidative degradation properties of the nanocomposites were found to be improved at a lower POSS–PLA content of 1–20 wt % and decreased at a higher content of 30 wt % compared to the neat PLA homopolymer. In addition, the cold-crystallization rates and crystallinities of the PLA/POSS–PLA nanocomposites became faster and higher, respectively, with increasing POSS–PLA content because of the nucleation effect of the POSS molecules tethered on POSS–PLA in the neat PLA matrix. The mechanical properties, such as the initial modulus and tensile strength, of the PLA/POSS–PLA nanocomposites were comparable with the neat PLA, regardless of the POSS–PLA content in the nanocomposites.

References

1. Lunt, J. Polym Degrad Stab 1998, 59, 145.
2. Drumright, R. E.; Gruber, P. R.; Henton, D. E. Adv Mater 2000, 12, 1841.
3. Ray, S. S.; Yamada, K.; Okamoto, M.; Ogami, A.; Ueda, K. Chem Mater 2003, 15, 1456.
4. Paul, M.-A.; Delcourt, C.; Alexandre, M.; Degee, P.; Monteverde, F.; Rulmont, A.; Dubois, P. Macromol Chem Phys 2005, 206, 484.
5. Chen, G.-X.; Kim, H.-S.; Park, B. H.; Yoon, J.-S. J Phys Chem B 2005, 109, 22237.
6. Jiang, L.; Zhang, J.; Wolcott, M. P. Polymer 2007, 48, 7632.
7. Singh, S.; Ray, S. S. J Nanosci Nanotechnol 2007, 7, 2596.
8. Yoon, J. T.; Jeong, Y. G.; Lee, S. C.; Min, B. G. Polym Adv Technol 2009, 20, 631.
9. Lichtenhan, J. D.; Otonari, Y. A.; Carr, M. J. Macromolecules 1995, 28, 8435.
10. Feher, F. J.; Wyndham, K. D.; Baldwin, R. K.; Soulivong, D.; Lichtenhan, J. D.; Ziller, W. J. Chem Commun 1999, 21, 1289.
11. Abe, Y.; Gunji, T. Prog Polym Sci 2004, 29, 149.
12. Romo-Uribe, A.; Mather, P. T.; Haddad, T. S.; Lichtenhan, J. D. J Polym Sci Part B: Polym Phys 1998, 36, 1857.
13. Zheng, L.; Farris, R. J.; Coughlin, E. B. Macromolecules 2001, 34, 8034.
14. Li, G. Z.; Wang, L.; Toghiani, H.; Daulton, T.; Koyama, K.; Pittman, C. U. Macromolecules 2001, 34, 8686.
15. Li, G.; Wang, L.; Ni, H.; Pittman, C. U., Jr. J Inorg Organomet Polym 2001, 11, 123.
16. Pyun, J.; Matyjaszewski, K.; Wu, J.; Kim, G.-M.; Chun, S. B.; Mather, P. T. Polymer 2003, 44, 2739.
17. Phillips, S. H.; Haddad, T. S.; Tomczak, S. J. Curr Opin Solid State Mater Sci 2004, 8, 21.
18. Markovic, E.; Matisons, J.; Hussain, M.; Simon, G. P. Macromolecules 2007, 40, 4530.
19. Ni, Y.; Zheng, S. Macromolecules 2007, 40, 7009.
20. Wang, J.; Ye, Z.; Joly, H. Macromolecules 2007, 40, 6150.
21. Kai, W.; Hua, L.; Dong, T.; Pan, P.; Zhu, B.; Inoue, Y. Macromol Chem Phys 2008, 209, 1191.
22. Lee, K. M.; Knight, P. T.; Chung, T.; Mather, P. T. Macromolecules 2008, 41, 4730.
23. Du, Y. J.; Lemstra, P. J.; Nijenhuis, A. J.; van Aert, H. A. M.; Bastiaansen, C. Macromolecules 1995, 28, 2124.
24. Kricheldorf, H. R.; Kreiser-Saunders, I.; Boettcher, C. Polymer 1995, 36, 1253.
25. Goffin, A.-L.; Duquesne, E.; Moins, S.; Alexandre, M.; Dubois, P. Eur Polym J 2007, 43, 4103.
26. Fina, A.; Tabuani, D.; Carniato, F.; Frache, A.; Boccaleri, E.; Camino, G. Thermochim Acta 2006, 440, 36.
27. Fina, A.; Tabuani, D.; Peijs, T.; Camino, G. Polymer 2009, 50, 218.